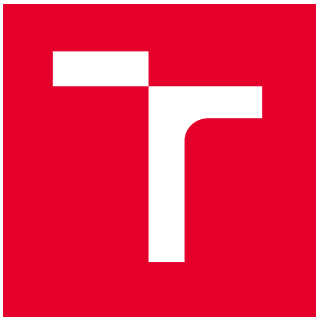

BRNO UNIVERSITY OF TECHNOLOGY

VYSOKÉ UČENÍ TECHNICKÉ V BRNĚ

FACULTY OF MECHANICAL ENGINEERING

FAKULTA STROJNÍHO INŽENÝRSTVÍ

INSTITUTE OF PHYSICAL ENGINEERING

ÚSTAV FYZIKÁLNÍHO INŽENÝRSTVÍ

ION SPECTROSCOPY FOR ANALYSIS OF SURFACE STRUCTURES

ION SPECTROSCOPY FOR ANALYSIS OF SURFACE STRUCTURES

DOCTORAL THESIS

DIZERTAČNÍ PRÁCE

AUTHOR — **Ing. Tomáš Strapko**

AUTOR PRÁCE

SUPERVISOR — **doc. Ing. Stanislav Průša, Ph.D.**

ŠKOLITEL

BRNO 2024

Abstract

The doctoral thesis deals with the fitting of spectra obtained by the Low-Energy Ion Scattering (LEIS) method. The algorithm, which is utilized nowadays, enables a stable analysis of the spectra, but it does not include, for their complexity, certain physical phenomena, which causes a consistent difference between experimental data and their fits. The algorithm, introduced in this work, attempts to describe the shape of the peaks and the background in the experimental data more accurately, utilizing the so-called L'Hoir peak.

Abstrakt

Doktorská práce se zabývá fitováním spekter získaných metodou nízkoenergiového rozptylu iontů - LEIS. Algoritmus, jenž se využívá v současnosti, umožňuje stabilní analýzu spekter, ale nezahrnuje v sobě, pro jejich komplexnost, některé fyzikální skutečnosti, což má za následek konzistentní rozdíl mezi experimentálními daty a jejich fitem. Algoritmus, představený v této práci, se snaží o přesnější popis tvaru píků i pozadí v experimentálních spektrech užitím takzvaného L'Hoirova píku.

Keywords

Low-Energy Ion Scattering, LEIS, spectra fitting, L'Hoir peak

Klíčová slova

Nízkoenergiový rozptyl iontů, LEIS, fitování spekter, L'Hoirův pík

Contents

Introduction

Technological advancements in the semiconductor industry, ceramics, etc. rely on reducing the dimensions of the respected parts or layers (transistors, ceramics), and enhance the importance of the surface. The purity, composition and thickness play crucial roles in the determination of the manufacturing process, storage and transportation.

The LEIS (Low-Energy Ion Scattering) method is the most sensitive experimental method for an analysis of the elemental composition of the outermost atomic layers. As probes, ions of noble gasses or alkali ions in primary energy range from 0.5 keV to 10 keV are impinging on the surface of the sample. After their backscattering from the surface towards the detector, the elements present on the surface are determined according to projectile's energy loss. Noble gasses are preferably used since they have a high probability of being neutralized after passing below the outermost layer [1] of the sample. When an electrostatic analyzer (ESA) is used, the signal from the deeper atomic layer is greatly reduced due to the choice of these projectiles. Experiments conducted for alkali metals as projectiles have been reported as well [2]. Low-Energy Ion Scattering has proven useful in a wide variety of samples, ranging from pure metals [3] to alloys [4].

In the presented work, we aim to discuss the procedure of extracting the information of interest from the ESA-LEIS spectra. The first part describes the basic principle of scattering interaction, probability of scattering occurrence and variant mechanisms of energy loss of the projectiles. Finally, the ESA-LEIS spectrum is described, highlighting the main contributions. The second part introduces the algorithm for spectra evaluation. The most utilized approach for spectral description is discussed and arguments for different approaches are listed. Next, various simultaneous investigations are presented in order to successfully utilize an alternative fitting method of LEIS spectra. Lastly, respected approaches are compared and issues with the latter approach are discussed.

The final part provides a mathematical foundation for the different approaches in fitting of the ESA-LEIS spectra.

Chapter 1

Theoretical part

1.1 Kinematics

Interaction between nuclei of projectile-target atom pair during the collisional event, neglecting the effects of interaction with neighbouring target's atoms as well as the influence of electronic orbitals of both participants, can be approximated by binary collision model. The collision is schematically depicted in Fig. 1.1.

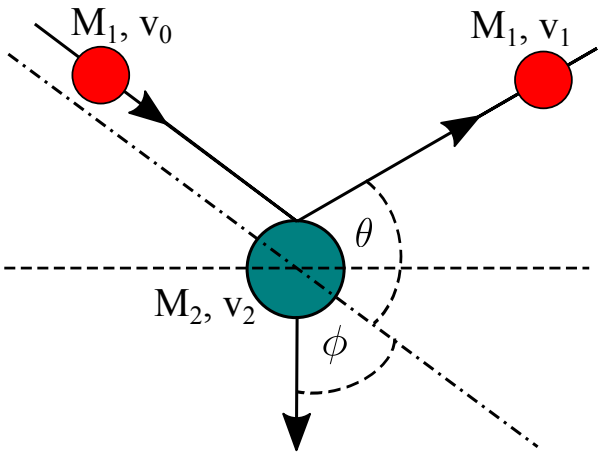

Figure 1.1: Binary model approximation. See [5] for comparison.

In the case of a static target atom with the mass M_2, momentum conservation law (in a parallel and perpendicular direction with respect to the incidence of the projectile) and kinetic energy conservation law [6]:

$$\frac{1}{2}M_1v_0^2 = \frac{1}{2}M_1v_1^2 + \frac{1}{2}M_2v_2^2, \tag{1.1}$$

$$M_1v_0 = M_1v_1\cos\theta + M_2v_2\cos\phi, \tag{1.2}$$

$$0 = M_1v_1\sin\theta - M_2v_2\sin\phi, \tag{1.3}$$

where M_1 is the mass of the projectile and v_0 its initial velocity. Scattering and recoiling angle θ and ϕ determine, for given projectile-target combination, the resulting velocities v_1 (projectile) and v_2 (target) [7].

Elimination of ϕ and subsequently v_2, a mutual fraction of resulting and initial velocity for the projectile is obtained:

$$\frac{v_1}{v_0} = \pm \frac{(M_2^2 - M_1^2 \sin^2\theta)^{1/2} + M_1 \cos\theta}{M_2 + M_1}. \tag{1.4}$$

In the case when $M_2 > M_1$, where the plus sign holds, the ratio stated above can be rewritten by means of kinetic energies as

$$E_1 = \left[\frac{(M_2^2 - M_1^2 \sin^2\theta)^{1/2} + M_1 \cos\theta}{M_2 + M_1}\right]^2 E_0 = kE_0. \tag{1.5}$$

The derived parameter, kinematic factor k represents a part of the initial kinetic energy E_0 of the projectile after the collisional event with the target atom's nucleus. As demonstrated in (Eq. 1.5), the value is straightforwardly determined from the projectile-target combination (masses of respected interacting particles) and the scattering angle of the projectile.

1.2 Atomic surface concentration and cross-section

The surface density n_S of the sample plays a crucial role in the probability of the collision between the projectile and the sample's atom, expressed as a ratio of incident N_i projectiles and projectiles scattered N_D into a differential solid angle $\mathrm{d}\Omega$ centered around scattering angle θ [7]. The connection between surface density and probability of collisional effect is given by differential scattering cross-section

$$\frac{\mathrm{d}\sigma(\theta)}{\mathrm{d}\Omega}\mathrm{d}\Omega \cdot n_s = \frac{N_D}{N_i} \tag{1.6}$$

In backscattering experiments, the solid angle of the detector is small, hence the cross-section can be written as

$$\sigma(\theta) = \frac{1}{\Omega}\int_\Omega \frac{\mathrm{d}\sigma}{\mathrm{d}\Omega}\,\mathrm{d}\Omega, \tag{1.7}$$

The scattering cross-section can be derived from the repulsive force acting during the collision. Deflected particles are treated as scatterers from an acting central repulsive force created by a point charge where the kinetic energy of the scatterers is preserved. A perpendicular distance between the path of the projectile and the line, parallel to its initial trajectory and passing through the target's nucleus is, denoted as impact parameter b. Parameter r_0 represents the distance of the closest approach during the scattering event. It plays a crucial role in the evaluation of charge-exchange processes (threshold energy, Sec. 1.9). Furthermore, the strength of interaction potential during a collision between projectile-target pair (Eq. 1.10) is also a function of this parameter.

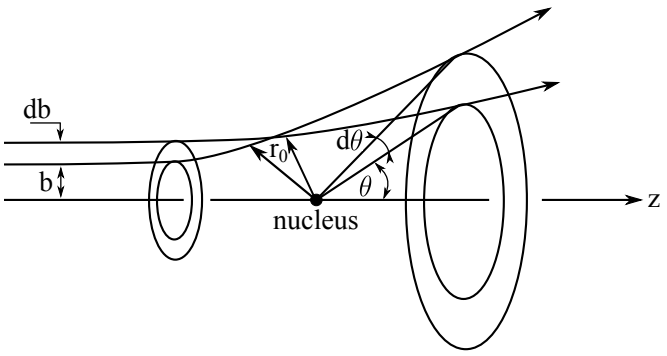

Figure 1.2: The influence of the impact parameter b on the scattering angle θ. The distance of the closest approach r_0 is depicted as well. See [7] for comparison.

Projectiles interacting with the nucleus in the interval $b+\mathrm{d}b$ will be deflected by the angle $\theta + \mathrm{d}\theta$. In central forces, there is a complete symmetry around the axis, henceforth

$$2\pi\, b\, \mathrm{d}b = -\sigma(\theta)\, 2\pi\, \sin\theta\, \mathrm{d}\theta. \tag{1.8}$$

(Eq. 1.8) describes cross-section as a relationship between the impact parameter and angular distribution after scattering from the nucleus. The minus sign indicates that scattering angle decreases for increasing impact parameter. The higher velocity of the projectile or larger impact parameter results in a smaller scattering angle.

1.3 Scattering potential

In High energy ion scattering experiments (HEIS; Rutherford backscattering, RBS) and Medium energy ion scattering (MEIS) the repulsive force acting between projectiles and target atoms is sufficiently calculated utilizing Coulomb potential of an atom with atomic number Z [5]:

$$V_C(r) = k\frac{Ze}{r} \tag{1.9}$$

with r being the distance from the atom's nucleus and k being the Coulomb constant. Low energy ion scattering, however, requires an introduction of scattering potentials that incorporate the effect of electron clouds screening between interacting nuclei, effectively weakening the Coulomb potential. The employed screening functions are solely dependent on the distance between projectile-target nuclei. Nowadays, screening functions proposed by Molière, derived from the Thomas-Fermi model of the atom (TFM) and Ziegler-Biersack-Littmark (ZBL) "Universal" potential are usually employed. Both functions are in the form of a sum of exponentials and the resulting screened scattering potential:

$$V(r) = V_C(r)\Phi\left(\frac{r}{a}\right) \tag{1.10}$$

is expressed as Coulomb potential multiplied by the screenig function $\Phi(r/a)$, where a is the screening length. The latter parameter is a function of the atomic number of the interacting particles.

1.4 Yield in LEIS

For experiments with an electrostatic analyzer (ESA), only projectiles that are charged pass through the energy analyzer and reach the detector. The yield of ions S_i scattered from an atom with mass M_i and its atomic surface concentration n_s is written as

$$S_i = \frac{I_t}{e} \cdot t \cdot \xi \cdot R \cdot \eta_i \cdot n_s \ , \tag{1.11}$$

where I_t represents an electrical current of primary ion beam, e is an elementary charge, t a total acquisition time, ξ is an instrumental factor (involving analyzer solid angle and efficiency and analyzer transmission), R represents a roughness factor of the surface and η_i is an elemental sensitivity factor, which is given by

$$\eta_i = \frac{S_i^+}{(S_i^+ + S_i^0)} \cdot \frac{d\sigma_i}{d\Omega} \ . \tag{1.12}$$

The expression $S_i^+/(S_i^+ + S_i^0)$, denoted as ion fraction P_i^+, is the ratio of projectiles in their charged state to the total yield of projectiles (ions and neutrals alike) after scattering from the sample's surface. The ion fraction will be discussed in detail in Sec. 1.6.

1.5 Stopping power

Dissipation of the kinetic energy of projectiles traversing through the sample occurs either via scattering events under small angles with nuclei of target's atoms [8], elastic (nuclear) energy loss, or via the interactions of electron clouds, inelastic (electronic) energy loss. The sum of these mechanisms is written as [7]

$$\Delta E = \Delta E_n + \Delta E_e \ . \tag{1.13}$$

Energy loss is proportional to the depth of penetration since the number of interactions between projectiles and atoms is increasing. Hence, an energy loss per the length of trajectory, stopping power, is defined

$$S = \frac{\mathrm{d}E}{\mathrm{d}x}, \tag{1.14}$$

usually expressed in eV/Å units. Identically to energy loss, stopping power is either nuclear or electronic.

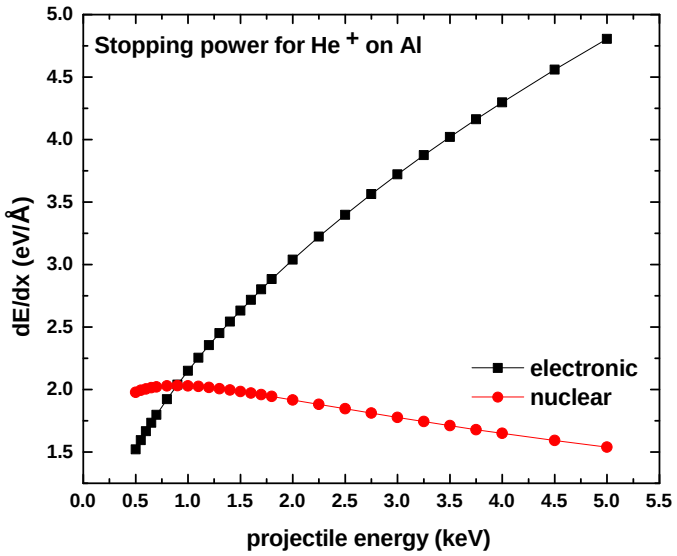

Figure 1.3: Comparison of nuclear and electronic stopping power for He-Al pair. For small energies, nuclear stopping becomes dominant. Data obtained from SRIM2013 [9] database.

Experimentally obtained data of stopping power are tabulated in SRIM2013 [9] database. An example for the low primary energies regime is shown in Fig. 1.3. Projectiles penetrating the sample with energy below 1.0 keV experience dominant stopping from interactions with the nuclei. To give an example, 1.0 keV He^+ projectile scattering from Al atom loses 2 eV of its kinetic energy when $\theta = 6.6°$.

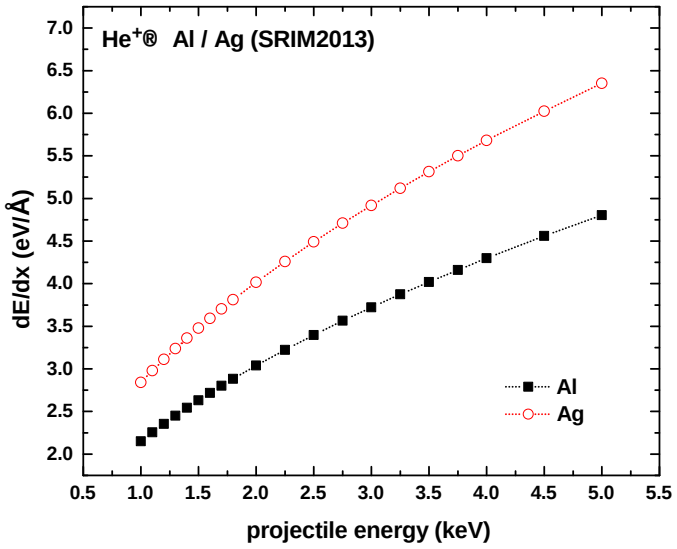

Figure 1.4: Electronic stopping power as a function of projectile's kinetic energy for He-Al and He-Ag pairs as tabulated in SRIM2013 [9].

Stopping power is a function of the target-projectile pair. An example of different values of electronic stopping power for He-Al and He-Ag pairs is shown inFig. 1.4. Transmission and backscattering experiments have been reported to result in different values of stopping power [10], which lead to a conclusion that electronic stopping is a function of impact parameter as well.

For a projectile, scattering under angle θ from the depth Δt, a schematical depiction of the energy loss mechanism is shown in Fig. 1.5.

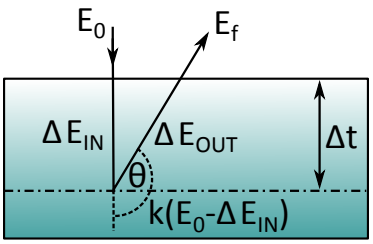

Figure 1.5: Schematic depiction of energy loss mechanism in binary approximation for a projectile scattering from the depth Δt in the sample.

Mathematically, in terms of energy losses, the final energy of the projectile is written as:

$$E_f = E_0 - \Delta E_{IN} - (1-k)(E_0 - \Delta E_{IN}) - \Delta E_{OUT}, \tag{1.15}$$

the term $(1-k)(E_0-\Delta E_{IN})$ denoting the energy loss after scattering under θ in the depth Δt, and terms ΔE_{IN} and ΔE_{OUT} representing the sum of energy losses while traversing along the sample's atoms, before and after scattering, respectively. For small penetration depths, valid in LEIS energies, $\Delta E_{IN} << E_0$, therefore the last bracket is close to one and the equation can be simplified to form:

$$E_f = kE_0 - (\Delta E_{IN} + \Delta E_{OUT}) = kE_0 - \Delta E_{total}. \tag{1.16}$$

The first term is identical with the scattering on the surface (Eq. 1.5). Hence, the signal from deeper layers has an energy offset from the signal originating on the surface by:

$$\Delta E_{total} = S_{e,IN}\Delta t + S_{e,OUT}\frac{\Delta t}{|\cos\theta|}, \tag{1.17}$$

where $S_{e,IN}$ and $S_{e,OUT}$ are values of electronic stopping power before and after collision, respectively. To give an example to support the claim of the performed simplification **??**, for He^+ projectiles with primary energy $E_0 = 3.0$ keV in aluminium (see further in the text), a particle scattering from the depth 10Å loses 37.2 eV, which is less than 2% of its primary energy E_0. Nuclear stopping power is not included, since the single-scattering event at depth Δt is assumed.

1.6 Charge-exchange processes

In experiments using an electro-static analyzer (ESA) [15], only projectiles that keep their charge after scattering from the sample are detected. Impinging ions therefore have to remain in their originally ionized state throughout the entire interaction, or undergo a series of events obtaining and losing the electron during their propagation. The final charge-exchange leads to reionization. For the case of metals, there are various types of charge-exchange mechanisms [1]:

a) *Resonant processes*
Transitions, proceeding via electron tunneling, in which only one electron is involved.

They can occur while the projectile is propagating in front of the sample's surface, between states in the target's conduction band (multiple target atoms are included) and weakly bound states of the projectile.

b) *Auger neutralization*
Transitions of charge involving two electrons from the target atom. For example, incoming He^+ projectiles could be neutralized directly to the ground state while a metal electron or plasmon is excited. In another possible mechanism, a metastable He atom is created, which then decays to a ground state, while a metal electron or plasmon is excited.

c) *Collision-induced processes*
Charge-exchange processes as an outcome of close interatomic distances between a single target atom and projectile. At a critical distance from the atom (and closer), the projectile can be either neutralized (collision induced neutralization, CIN) or reionized (collision induced reionization, CIR). The latter manifests in step-like behaviour - in case of an approaching He^+ projectiles, the probes undergo a transition $He^+ \xrightarrow{+e} He^0 \xrightarrow{-e} He^+$ and lose $\Delta E_{(\mathrm{He})\to CIN\to CIR}\,(\mathrm{He}) \sim 20\,\mathrm{eV}$ [16].

A resulting ion fraction (see the first fraction in (Eq. 1.18)) when collisional effects are included is written as [1], [13]

$$P^+ = P^+_{in} \cdot (1 - P_{CIN}) \cdot P^+_{out} \,+\, (1 - P^+_{in}) \cdot P_{CIR} \cdot P^+_{out}\,, \tag{1.18}$$

where P^+_{in} and P^+_{out} denote the survival probability of the incoming and outgoing projectiles, respectively. The first term describes the ion survivals, i.e. projectiles that scattered towards the detector and survived both CIN and Auger neutralization. The second term describes the reionized particles - after Auger neutralization, probes lose their electron via CIR and are not neutralized on their outgoing trajectory.

1.7 IONTOF Qtac^{100}

All data presented in this work have been obtained by High Sensitivity Low Energy Ion Scattering (HS-LEIS) instrument Qtac^{100} from IONTOF GmbH company. The instrument is a part of the UHV cluster located in CEITEC Nano facility in Brno. The main distinguishing feature of Qtac^{100}, compared to the usual experimental LEIS systems, is its analyzer, collecting particles over the entire azimuthal angle. Hence, the sensitivity of the analysis is significantly enhanced. Moreover, the acceptance angle of the analyzer, $\xi = \pm 0.2°$, allows only a narrow range of backscattered projectiles to enter the detector. The peak resolution is, therefore, improved as well. The schematic cross-section of Qtac^{100} system is shown in Fig. 1.6.

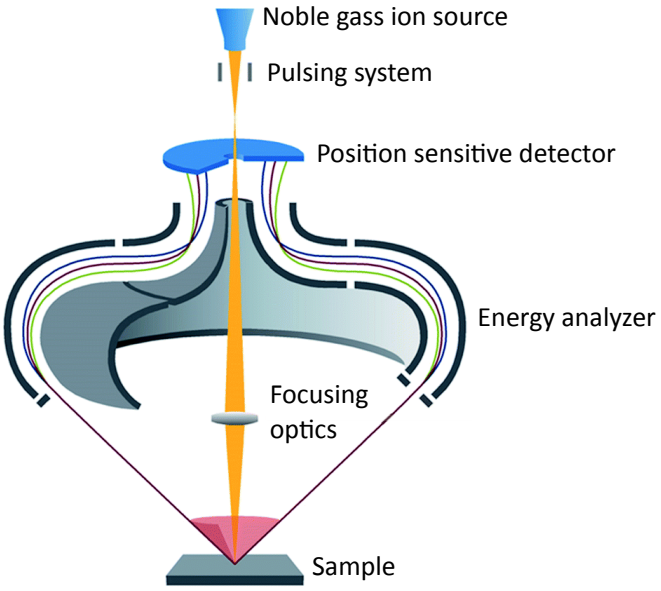

Figure 1.6: Schematic cross-section of Qtac^{100} from IONTOF GmbH company. Obtained and adjusted from [17].

The projectiles are impinging perpendicularly on the sample's surface. After backscattering under 145° scattering angle, they are passing through an energy analyzer, where their trajectory is curved according to their final kinetic energy after the last collision. Only charged particles pass through the analyzer, hence the instrument utilizes the ESA-LEIS method.

1.8 LEIS spectrum

A signal in LEIS, using an electrostatic analyzer, consists, in general, of 4 main contributions:

I) *Surface peak* - a part of the spectrum containing a signal of projectiles experiencing only one scattering event, described via kinematic factor (Eq. 1.5) in binary collision approximation, directly representing the elemental composition of the outermost atomic layers of the sample. In general, the surface peak protrudes from the rest of the spectrum, as visible in Fig. 1.8. For cases of clean metals, on the other hand, a surface peak is almost exclusively formed by these particles, with negligible contribution from the rest of the signals in the spectrum, see **??**. Part of the surface peak signal formed by particles experiencing exclusively single-scattering events is called the **binary peak**.

II) *Multiple-scattering regime (MS regime)* - projectiles experiencing a number of collisions in the outermost atomic layers, which emerge in the spectrum with final energy higher than the one predicted by the kinematic factor for a single scattering event. According to binary collision approximation, if the projectile experiences $n > 1$ collisional events and the sum of respected scattering angles ν_i equals the scattering angle of the analyzer, $\theta = \sum_i \nu_i$, then the final kinematic factor is written as $k_{MS} = \prod_i k(\nu_i)$ and could result in a number larger than kinematic factor for a single binary collision (forming the binary peak), $k_{MS} > k(\theta)$. Depending on the trajectory and depth of penetration within the sample, i.e. energy loss due to stopping power, the final energy of such projectile can surpass that of projectile scattered only once on the surface of the sample [5], [11].

III) *Reionization background* - particles interacting below the outermost layer while their charge state is altered (see Sec. 1.6). These particles experienced multiple-scattering events, but in contrast to category II, they originate from deeper layers where different physical phenomenons apply.

IV) *Sputtered background* - albeit LEIS is often referred to as a non-destructive experimental method, atoms from the top of the sample can be sputtered from their original position and reach the detector. This kind of background, produced by secondary particles, is often referred to as SIMS (Secondary Ion Mass Spectroscopy) background [11].

The listed scattering mechanisms are shown in Fig. 1.7. In the experimental spectra, these phenomenons manifest according to the depiction in Fig. 1.8.

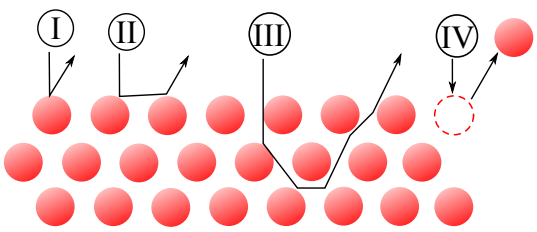

Figure 1.7: Respected scattering mechanisms, I - III, and sputtering events, IV, occurring during LEIS experiments. The projectiles and the secondary sputtered particles are leaving the surface in the direction of the energy analyzer.

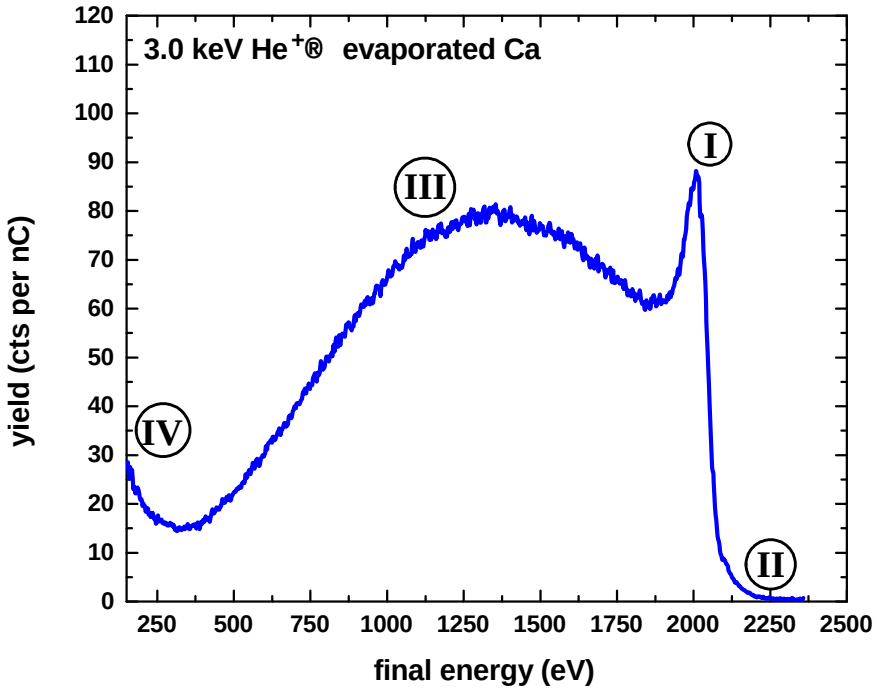

Figure 1.8: Respected physical phenomenons generating contributions to the overall shape of the LEIS spectrum for 3.0 keV He^+ projectiles impinging on evaporated Ca sample. Surface peak (I), located at 2000 eV, protrudes from the rest of the spectrum. Multiple-scattering regime (II) is also present. Calcium is very effective in the reionization of He^0 projectiles [11], thus the reionization background (III) is extraordinarily strong. The signal of sputtered particles (IV) is present for final energies below 330 eV.

To describe respected regimes, the following functions have been widely accepted within the LEIS community:

a) **gaussian function** for evaluation of projectiles forming **binary peak**, part of surface peak (I) experiencing only one single-scattering event;

b) **exponential decay** for approximation of the *sputtered (SIMS) background* (IV);

c) **error function**, **ERF**, for fitting of both *multiple-scattering (MS) regime* (II) and *reionization background* (III).

In this work, we focus on spectra, where the sputtering background, IV, does not interfere with the surface peak, hence from this point on, we restrict our fitting attempts only to the scattering mechanisms I - III. The borders between respected regimes are not strictly determined, the signals overlap. A successful determination of the binary peak is crucial for the subsequent quantitative analysis of the samples.

1.9 The choice of the samples

Fitting methods in the following chapters are mainly applied on spectra of aluminium foil, since aluminium has only one naturally occurring stable isotope, measured by He^+

projectiles in energy range (1.0 - 4.8) keV. With increasing primary energy E_0 of the projectiles, the reionization background and multiple-scattering regimes are more profound, relative to the surface peak, since projectiles with higher velocities penetrate deeper within the sample, see Fig. 1.9.

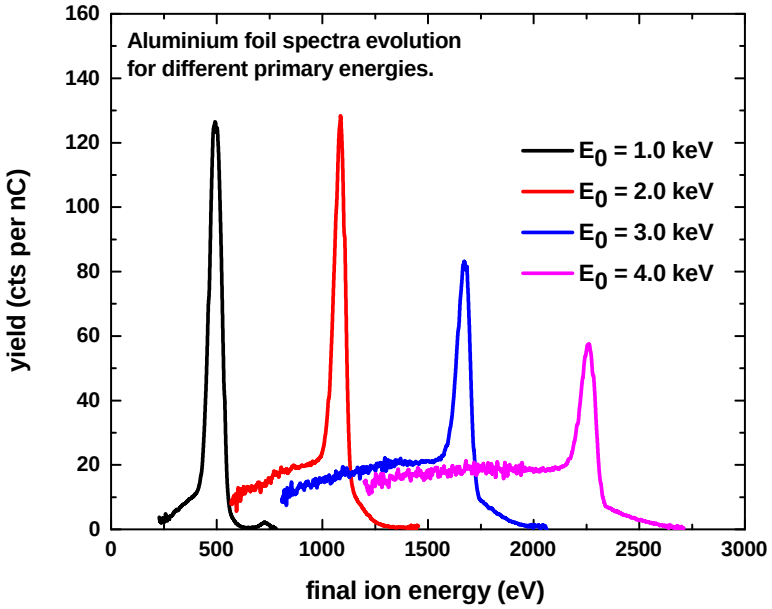

Figure 1.9: Evolution of ESA-LEIS spectrum for He^+ on Al foil for different primary energies obtained by Qtac[100] instrument. Increasing of the reionized background as well as MS regime, relatively to the surface peak, with higher E_0 is clearly visible.

1.10 Simulations of ion collisions in solids

Mechanisms of the collisional events occurring during the interactions of projectiles impinging on the sample are stochastic. Although an analytical approach is possible for certain cases [8], simulations offer more detailed insight into the behaviour of scattering events. Various software can be utilized, depending on the experimental conditions - incident angle, scattering angle, acceptance angle of the detector and sample's structure. In the case of LEIS experiments for polycrystalline samples, TRBS [19] (Transport for Rutherford Backscattering) is a viable simulation tool. It is a software derived from TRIM (Transport of Ions in Matter) with improved computational speed, at the expense of being able to simulate only perpendicular incidence, with respect to the surface plane. The software enables to collect signals from different layers, as well as the contribution of particles experiencing different numbers of collisions, utilizing Monte Carlo simulations for computing the scattering events, collecting both ions and neutrals - charge integrated spectra [20]. The acceptance angle of the detector in TRBS simulation can be varied, however, the particles collected in the entire azimuth are analyzed, exactly like in experiments using Qtac[100] instrument. It is, however, not possible to simulate the data of ion yields directly, since the general formula for the reionization function has not been proposed yet. In Subsec. 2.2.5 more details are provided.

Chapter 2

Practical part

2.1 Algorithm description

Evaluation of the data in this work is performed by *Matlab R2014a* script, utilizing some of the built-in functions. Spectra are smoothed by the Savitzky-Golay algorithm of 3rd order with the number of frames corresponding to the value where the difference between the center of the surface and smoothed peaks does not exceed 8 eV. The next step is to perform a numerical derivation from the left to locate the peaks within the spectrum. A simple determination method is executed: every positive peak in the derivation spectrum must have its negative counterpart. Since the area of surface peak is of interest, a reasonable part of the spectrum surrounding the peak should be taken into consideration. Hence, the algorithm proceeds with an automatic choice of two inflex points from each side of the peak. Due to a bump in the smoothed spectrum, see Fig. 2.1, the right inflex point, which is a by-product of the Savitzky-Golay smoothing algorithm, is sometimes evaluated suboptimally. This situation mainly occurs in the case of spectra with a very low background. It needs to be stressed that the described algorithm is run solely to determine the inflex point from both sides of the experimental peaks. A subsequent fitting process is performed for the original dataset, with an exception discussed in Subsec. 2.2.4.

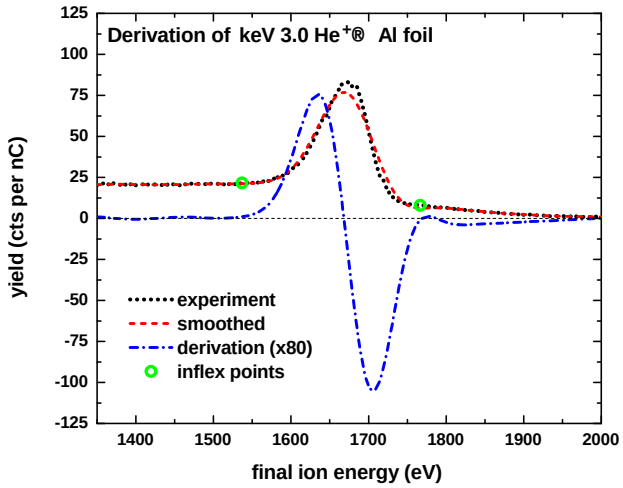

Figure 2.1: Original (black dot) and smoothed (red dash) dataset. Numerical derivation of the latter (blue dash-dot) determines the inflex points for subsequent evaluation (green circles).

2.2 Methods of spectra fitting

2.2.1 Gaussian function + Error function

In Sec. 1.8, a standard method for evaluation of binary peak was introduced. This method represents the most robust and quickest approach to evaluating the area of the binary peak in the surface peak. It is based on a mutual combination of Gaussian curve [13], [21], approximating the binary peak, and error function, ERF, representing the signal from deeper layers, reionization and MS regime alike. Its shape is modulated according to the shape of LEIS spectra from both sides of the surface peak

$$f(E) = b_1 + m_1 E + (b_2 - b_1 + (m_2 - m_1)E) \cdot \frac{1}{2}\left[1 + \ \mathrm{erf}\left(\frac{E-\mu}{\sigma}\right)\right], \qquad (2.1)$$

where $b_{1/2}$ and $m_{1/2}$ are offsets and slopes of linear functions approximating the background shape. Parameters σ and μ are the standard deviation and center of the distribution of Gaussian and Error functions.

The idea of the ERF, proposed by Rik ter Veen (TASCON GmbH), originated from the convention of describing the signal in LEIS spectra from a single atomic layer by Gaussian curve. Therefore, the contribution of adjacent layers can be described by the multitude of Gaussians with shifted centers. Their sum (ERF) reasonably approximates the background shape in the close vicinity of binary peak. The position of the center of ERF, with respect to the position of the binary peak, is a function of reionization energy loss and electronic stopping power. While the first mechanism of energy dissipation has a constant value of ~ 20 eV, see Sec. 1.6, the latter depends on the primary energy of the particle and the distance between the layers in the sample as well, compare with Sec. 1.5. Since it is difficult to correctly predict the distance for polycrystalline samples (more in Subsec. 2.2.6) the center of ERF was kept as 30 eV towards left from the center of surface peak during the fitting procedure for the analysis of all samples and primary energies.

Utilization of the combination of the Gaussian curve and ERF is shown for 3.0 keV He^+ projectiles impinging on the Al foil in Fig. 2.2. This fitting procedure fails to reproduce the MS regime from 1850 eV towards higher energies. Moreover, the fit fails to accurately describe the shape of the experimental spectrum, namely at the high and low energy edges of the surface peak, where the experimental data are underestimated from the left and overestimated from the right side. The position of the surface peak is shifted towards lower energies as well, hence the tip of the peak is not approximated accurately either. The difference between the experiment and fit above 1925 eV towards higher energies is caused by the slope of ERF calculated in the closer vicinity of the surface peak.

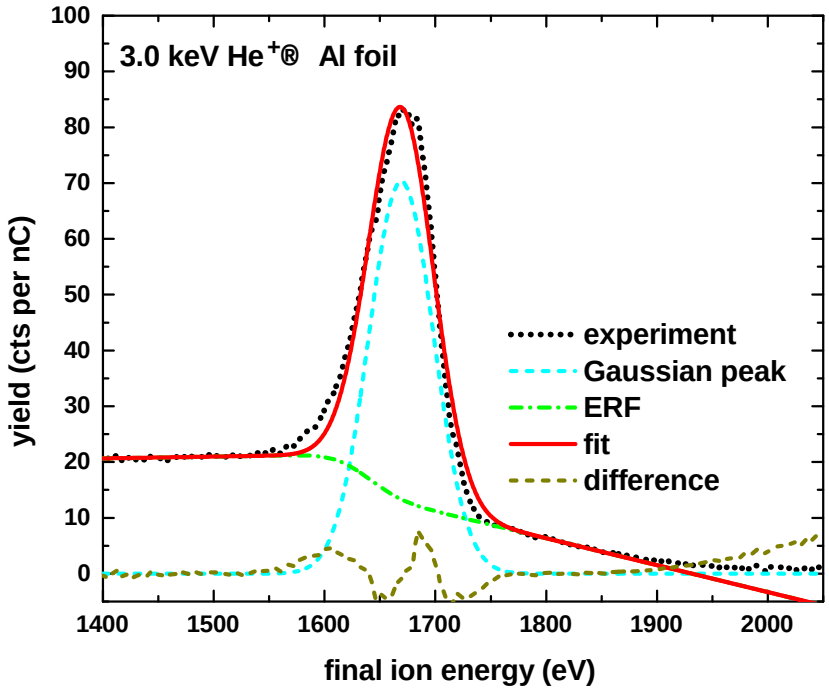

Figure 2.2: Example of the fit for LEIS spectrum with strong multiple-scattering regime, 3.0 keV He^+ on Al foil. Fit (red solid) is a combination of Gaussian peak (cyan dashed) and ERF (green dashed-dotted). A visible difference (dark yellow dashed) from the experimental data (black dotted) is observed at both high (above 1725 eV) and low (below 1625 eV) sides of the surface peak. Moreover, the fitted binary peak is slightly shifted towards lower energies.

The described fitting procedure is very robust. Width, σ, and position (center), μ, of both functions are the only 4 parameters required for the fit. In addition, fixing the mutual shift between them by 30 eV, only 3 parameters are required: width and position of Gaussian function and width of ERF.

2.2.2 Asymmetric response

In experiments under grazing scattering angles [22], a prolonged low-energy edge of the experimental peak was observed, as a result of ions remaining in close proximity to the sample's surface for sufficient amount of time so that electronic stopping power took pronounced effect. The perpendicular distance from the sample's surface, where electronic stopping begins to influence the energy of the projectile, is attributed to the distance where the electron density of the outermost sample's electrons becomes identical with the bulk density, d_s. According to findings in [23], for Al (111) surface $d_s \sim 2$Å. This is the fundamental principle of friction coefficient theory [24]. The kinematic factor plays, virtually, no role in the chosen experimental set-up. Resulting peaks were described as a convolution of Gaussian – straggling – and exponential decay – electronic stopping power. Albeit the data in the paper were collected foremostly for He^{2+} primary projectiles, the peak shape for He^+ projectiles is only slightly thinner.

For experiments with perpendicular geometry, the kinematic factor becomes a major influence. Electronic stopping has less time to act upon the passing projectiles, and its value changes after the violent scattering event between the projectile and the target [25].

As an example, He^+ projectile with primary energy 3.0 keV experiences $S_e = 3.72$ eV/Å. After collision under scattering angle $\theta = 145°$ on Al atom, the value of electronic stopping power drops to $S_e = 2.82$ eV/Å. The principle of the energy loss, excluding reionization processes, remains, however, the same as for the grazing angle experiments. The difference between experiments is shown in Fig. 2.3. For grazing experiments in [22], the trajectory parallel with the sample's surface was taken into consideration (incident and scattering angles were small), whereas for the perpendicular experiment, the entire trajectory has to be included (Eq. 1.17).

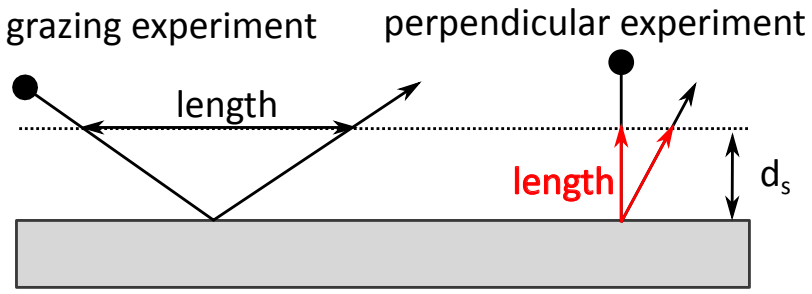

Figure 2.3: Comparison between grazing and perpendicular experiment.

2.2.3 L'Hoir peak + Error function

Taking the arguments from the previous subsection into consideration, a different peak shape, the result of a convolution of the Gaussian function **??** and an exponential function in a form [26]:

$$f(E) = \exp\left(\frac{\mu}{\tau}\right) H(-\mu) \tag{2.2}$$

where $H(-\mu)$ is a Heaviside step function, resuls in so-called **L'Hoir peak** [27]. The described distribution shows a possibility of promising utilization in the process of fitting the LEIS spectra. Analytical expression of L'Hoir peak:

$$f(E) = A \cdot \exp\left(\frac{E-\mu}{\tau}\right) \mathrm{erfc}\left[\frac{1}{\sqrt{2}}\left(\frac{E-\mu}{\sigma} + \frac{\sigma}{\tau}\right)\right], \tag{2.3}$$

introduces only one additional parameter of the fit, skewness τ. Within this parameter, the asymmetry of the binary peak is included. The complementary error function is numerically inverse function to ERF, $\mathrm{erfc}(x) = 1 - \mathrm{erf}(x)$. Improvement of the data approximation with MS regime is shown in Fig. 2.4. In the vicinity of the peak, the fit slightly overestimates the left part of the experimental peak, around 1590 eV.

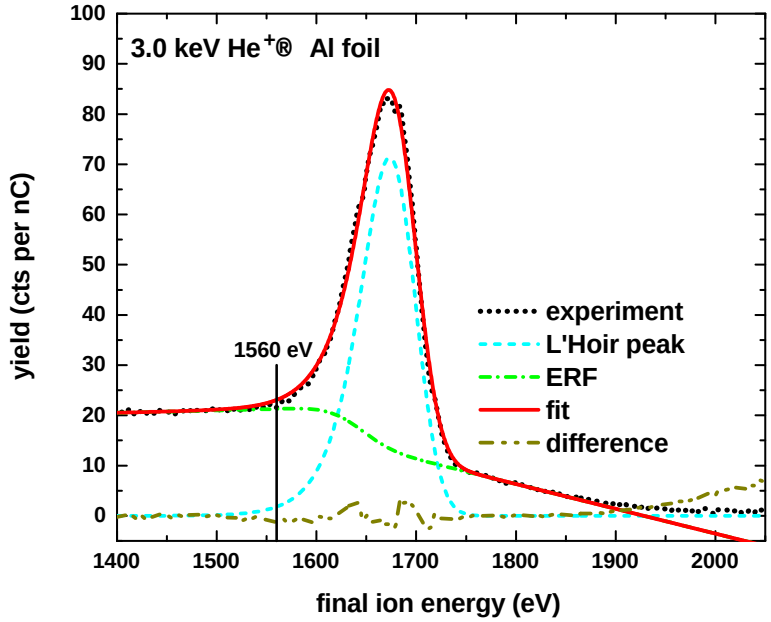

Figure 2.4: Example of the fit for LEIS spectrum with strong multiple-scattering regime, 3.0 keV He^+ on Al foil. Fit (red solid) is a combination of L'Hoir peak (cyan dash) and ERF (green dash-dot). A difference (dark yellow dash) from the experimental data (black dot) is significantly reduced, compared to previous case in Fig. 2.2. Only minor discrepancy between experiment and fit can be observed around 1560 eV. The difference above 1925 eV remains the same. Description of the surface peak is almost perfect, a slight disagreement is observed due to an artifact resulting by the data acquisition in Qtac[100].

The described fitting procedure is very robust, similar to the previous fitting approach. Only 4 parameters (for the fixed shift between L'Hoir and ERF) are required: width, position and skewness τ of L'Hoir peak and width of ERF.

A good agreement between experimental data and fit might lead to a conclusion that no further attempts at the description of LEIS spectra are needed. However a subsurface signal requires more attention. Furthermore, despite its practicality, ERF, in both listed fitting methods, approximates two different physical mechanisms, namely reionization background and MS regime. To investigate the shape and intensity of possible subsurface signals contributing to the resulting form of the surface peak, additional analysis is made in the following sections.

2.2.4 Deconvolution of Al spectra

The strong contribution of the MS regime in the spectrum is an outcome of deeper atomic layers being visible to the probing ion beam. For this reason, a signal from this part of the sample to the surface peak should not be automatically neglected or included in the fit by the Gaussian (L'Hoir) peak for a single-scattering event at the surface. To investigate the phenomenon, Van Cittert (- Jannson) [28], [29] deconvolution algorithm was applied on spectra of 3 keV He^+ impinging on Al foil sample, as shown in Fig. 2.5.

Utilizing the deconvolution algorithm, experimental data have to be smoothed in order to eliminate sharp edges in the spectrum. As a response function, the Gaussian peak was opted for, since it requires only σ parameter to be adjusted. The position of the binary

peak (and the rest of the signals) is found by the iterative algorithm itself. To obtain shown results, a number of iterations $k = 3.5 \cdot 10^5$ was chosen and the width of the Gaussian response, derived from the experimental data, was gradually decreased. A very close approximation of the smoothed data was found for a wide range of widths, σ, of the Gaussian function. However, these fits produced a bump in the reconstructed background around 1700 eV. To compensate for this phenomenon, parameter σ was further decreased until this bump was eliminated, resulting in different intensity and position of the binary peak.

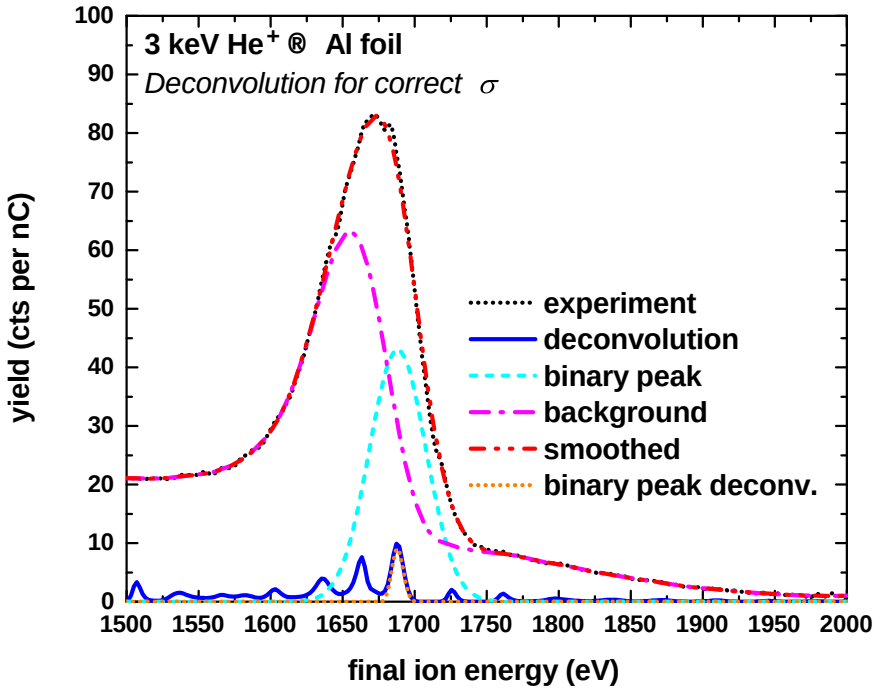

Figure 2.5: Deconvolution for fixed Gaussian spread function applied on 3.0 keV He^+ impinging on Al foil. Before the deconvolution algorithm is utilized, a smoothing of the experimental data is required (red dash-dot-dot). Deconvolution amplitudes (blue solid) represent the decoded signals in the smoothed spectrum. The amplitude representing the signal of the binary peak (orange dot) at 1687 eV was selected from the rest of the amplitudes by simple linear subtraction: from each side of the peak, a first local minimum was found. Then a linear function was fitted between these points and the area below it was subtracted. The values above and below local minima were set to zeros. The reconstructed binary peak (cyan dash) was obtained by convolution of the response Gaussian function and a selected peak in the deconvolution signal. The resuming background (magenta dash-dot) was reconstructed by the same method, excluding the selected peak.

The respected scattering regimes forming the overall background, reionization background and MS regime, are fused in the presented analysis. As mentioned in Sec. 1.8, these signals are overlapping. For this reason, the deconvolution algorithm struggles to recognize one from the other. In both figures, the surface peak is predominately formed by the combination of these contributions. Their total sum reaches the maximum value around 1650 eV.

2.2.5 TRBS simulations

Results from the deconvolution algorithm suggest that a significant part of the surface peak in LEIS spectra with a strong MS regime is formed by particles experiencing different collisional mechanisms than single-scattering events. Henceforth, an investigation implementing a physical model has to be introduced to eliminate the risk of being led astray by the shape-based algorithm itself.

As stated in Sec. 1.10, direct simulations of Qtac^{100} data for thick samples are not possible, since for these experiments, only ions are collected, whereas charge-sensitive simulations are not yet available. For this reason, we divided the surface into thin layers to determine the depth from which the signal of interest originates. Simulation setup matched the experimental conditions of Qtac^{100} system: scattering angle $\theta = 145°$ and acceptance angle $\xi = \pm 0.2°$. Spectrum for 3.0 keV He^+ projectiles on Al was simulated. Electronic stopping power for the He-Al pair was adjusted according to the SRIM2013 database, hence correction $c_e = 1.611$ was applied. The cut-off angle was set to $\sim 15°$ to keep the mean number of collisions close to 10 collisions per layer. The total thickness of the Al sample was set to 1500Å: since no particles were transmitted for a chosen set of parameters, it could be considered as an infinitely thick sample. Interatomic strength was screened by TFM potential.

In [30], the surface of a polycrystalline sample of copper, face-centered cubic crystal structure (the same as for Al) is described as (111) facets stacked upon each other. Considering the structure for (111) crystal direction, three atomic layers are visible for an incoming ion beam, as shown in Fig. 2.6.

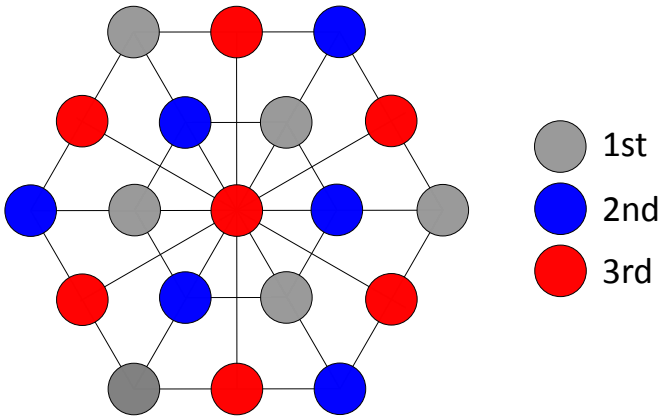

Figure 2.6: Visible atomic layers of (111) direction in Al crystal.

The interplanar distance in (111) direction, for lattice parameter of aluminium $a_{Al} = 4.05$Å, equals $d = a_{Al}/\sqrt{3} \approx 2.34$Å. Hence, a thin 4.68Å aluminium layer, corresponding to a interplanar distance between the first and the third atomic layer in (111) direction, was simulated to see the distribution of particles backscattering from the sample's surface. To match the height and width of the experimental spectrum, a series of simulations with different thicknesses of Al layers were performed. A layer with 11.7Å thickness, corresponding to 5 interplanar distances in (111) direction, was found to approximate Qtac^{100} data with very good accuracy when combined with ERF of adequate width and shift from the binary peak, as shown in Fig. 2.7.

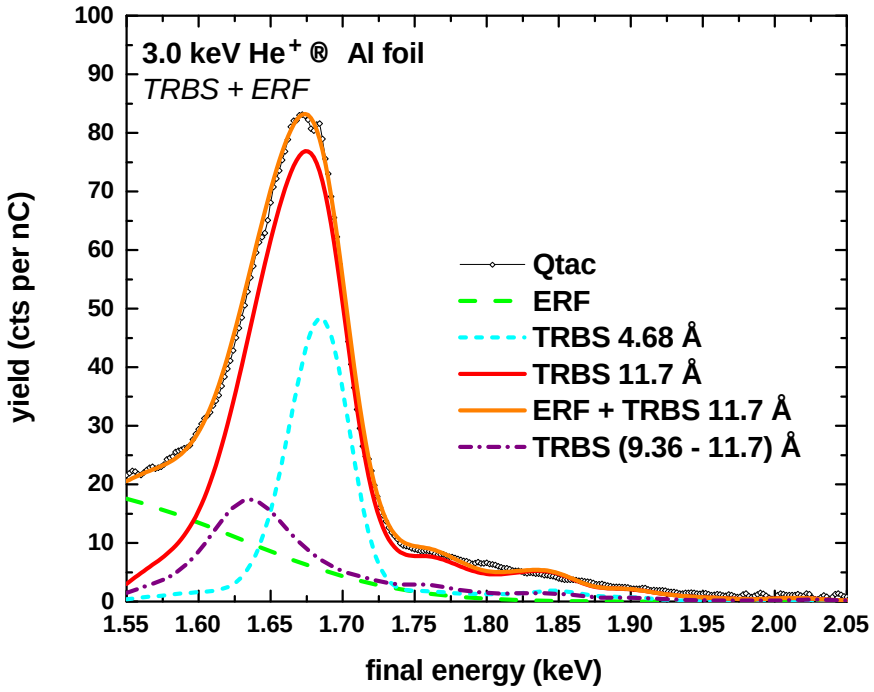

Figure 2.7: Comparison of Qtac[100] experiment (black open symbol) and TRBS simulation of 11.7Å thick layer (red solid). A thin 4.68Å layer (cyan dash) contributes less significantly to the resulting shape of the surface peak. Simultaneously, the majority of this signal is expected to be formed by projectiles experiencing binary collisions, since the signal from either side of the peak is low. Overall fit, as a sum of ERF (green dash) and 11.7Å layer overestimates the experimental data from the center of the surface peak towards lower energies. The expected contribution of MS particles to the surface peak (magenta dot) is a product of subtracting ERF and 4.68Å layer from Qtac data. The 5th layer (violet dash-dot) significantly overlaps with the ERF.

The width of the right edge of the surface peak for the original TRBS simulation was adjusted to match the width of the experimental surface peak. To adjust the height of the TRBS spectrum, the areas below the MS regime of experiment and simulation from 1725 eV to 1900 eV were equalized. It is visible that the TRBS signal from thin 4.68 Å layer consists, predominantly, of particles that experienced only one scattering event, since the background from either side of the peak is very low. However, due to the presence of MS particles, a depicted signal cannot be considered as binary peak, since the subtraction of the background is required. The center of ERF was shifted towards lower energies, taking into consideration two mechanisms of energy dissipation.

One part is attributed to the energy loss caused by collision-induced process for He projectile $\Delta E_{(\mathrm{He}^+)\to CIN\to CIR}\,(\mathrm{He}) \sim 20\,\mathrm{eV}$ (compare with Sec. 1.6), while the rest is attributed to electronic stopping power, tabulated in SRIM2013 database, so the energy loss (Eq. 1.17) is calculated as:

$$\Delta E_{total} = d_{IN}\cdot S_{e,IN} + d_{OUT}\cdot S_{e,OUT} = 4.68\cdot 3.72 + \frac{4.68}{\tan 35^\circ}\cdot 2.82 \approx 36\ \mathrm{eV}, \qquad (2.4)$$

where d_{IN}, d_{OUT} is the length, in Å, of the incoming and outcoming trajectory of the projectile scattering from the depth of 4.68 Å from the theoretical first atomic layer on the surface. Experimentally obtained (SRIM2013 database [9]) values $S_{e,IN}$, $S_{e,OUT}$ are corresponding electronic stopping powers in eV/Å. In total, the centre of ERF is shifted

by $\Delta E_{binary-ERF} = \Delta E_{(\mathrm{He}^+)\rightarrow CIN\rightarrow CIR} + \Delta E_{total} \sim 56\,\mathrm{eV}$, with respect to the center of the 4.68 Å (cyan dash) thin layer around 1684 eV. The width of ERF equals $\sigma_{ERF} = 3.5 \cdot \sigma_{surface\ peak}$. For the presented case, the fitted area from the left side of the surface peak is reduced, hence ERF remains horizontal, contrary to approaches discussed in Subsec. 2.2.1 and Subsec. 2.2.2. Hence, the analysis does not rely on the shape of the background in the vicinity of the surface peak.

The shape of ERF was empirically adjusted to fit the experimental LEIS data as closely as possible when paired with the discussed TRBS simulated layer.

Concerning scattering events at the surface, in Fig. 2.8, 3 keV He^+ on Al foil, an expected MS regime (magenta short dash-dot), forming the experimental spectrum, is outlined. It is a contribution, predicted by TRBS, from 4.68 Å to 11.7 Å. It has to be mentioned that 4.68 Å thin layer also includes part of the total MS regime since it exhibits a low background from both sides of the peak. Hence, to describe the MS regime in its complexity, this signal has to be included as well.

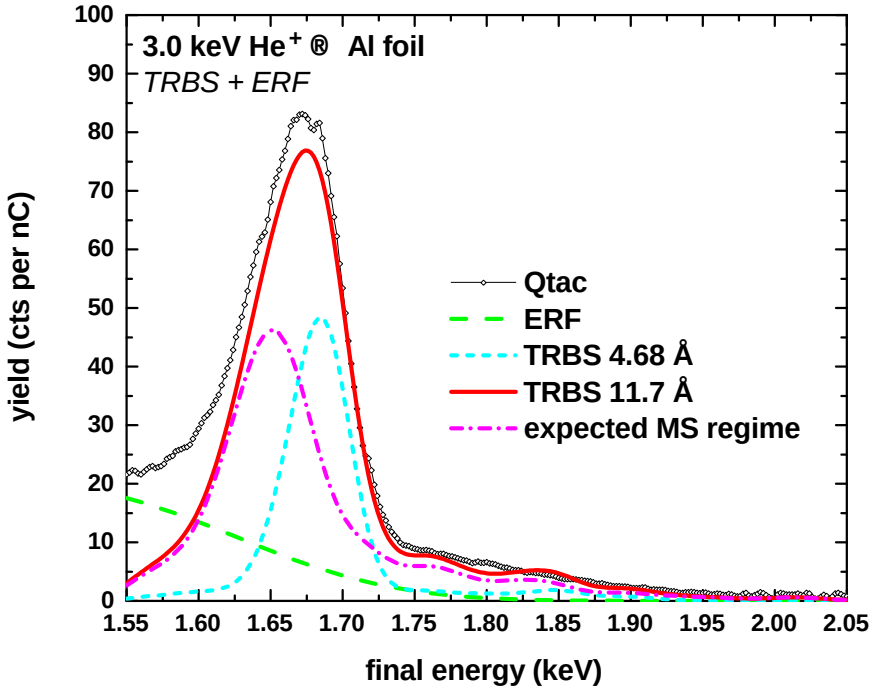

Figure 2.8: Part of the simulated spectrum describing the expected contribution of the MS regime to the experimental spectrum. For presented case, a signal from 4.68 Å to 11.7 Å is shown. It has to be mentioned that 4.68 Å thin layer also includes part of the total MS regime since it exhibits a low background from both sides of the peak. Hence, to describe the MS regime in its complexity, this signal has to be included as well.

2.2.6 Multiple-scattering approach

Approaches discussed in the two previous sections henceforth lead to a similar conclusion - the strong contribution of the MS regime in LEIS spectra non-negligibly reduces the signal of single-scattered particles in the resulting binary peak. Taking this phenomenon into consideration, we propose the following approach to fitting the LEIS data:

a) the signal from the surface is not strictly bound to the single atomic layer, hence the binary peak is skewered towards lower energies, as discussed in Subsec. 2.2.5;

b) the center of ERF is shifted, with respect to the position of the binary peak, according to the electronic and reionization energy loss;

c) the signal of the MS regime is modeled by the mutual combination of Gaussian function and inverse L'Hoir peak - its exponential decay is directed towards higher energies.

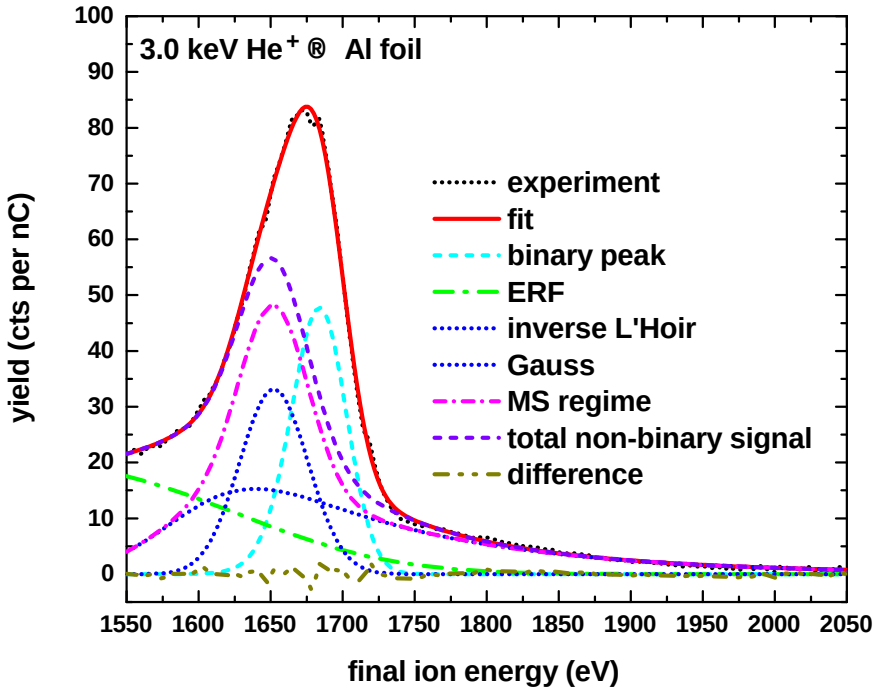

Figure 2.9: Experimental spectra from 3.0 keV He^+ on Al foil fitted by L'Hoir peak (cyan dash), ERF (green dash-dot) and mutual combination (magenta short dash-dot) of inverse L'Hoir and Gaussian peaks (blue dotted). The total non-binary signal (violet dash) is a mutual combination of the MS regime and ERF. The width of ERF was kept at $\sigma_{ERF} = 3.5 \cdot \sigma_{surface\ peak}$, the same as in the TRBS investigation. Discrepancy between the measured data (black dot) and fit (red solid), in practical terms, vanishes.

Incorporating these functions into the fitting procedure in Matlab, utilized in Subsec. 2.2.1 and Subsec. 2.2.3, for 3.0 keV He^+ on Al foil gives the results shown in Fig. 2.9. MS regime is fitted by a mutual combination of inverse L'Hoir and Gaussian peaks. In combination with the ERF, the total non-binary signal contributes to the majority of the surface peak. The signal of the binary peak is significantly reduced, in comparison with previously discussed fitting methods, following the results from an investigation of deconvolution and TRBS approaches. Reionized background, represented by ERF, is shifted towards lower energies by $\sim 56\,\mathrm{eV}$, and its width $\sigma_{ERF} = 3.5 \cdot \sigma_{surface\ peak}$, the same as in the TRBS investigation. The difference between experiment and fit, practically, vanishes. The

fitting area from the left of the binary peak is reduced, compared to previously discussed approaches. The combination of inverse L'Hoir peak and ERF would fail to predict the background shape further from the surface peak, hence the extension towards lower energies is determined by the left inflex point, discussed in Sec. 2.1. We propose to denote this fitting procedure as the **multiple-scattering approach** since the combination of the inverse L'Hoir and Gaussian is utilized to approximate the MS regime, following the shape outlined by TRBS simulations.

The closest fits of MS regime for the entire investigated energy range were found for $\sigma_{ERF} = 1.5\sigma_{surface\,peak}$. Henceforth, we will adhere to this value of ERF width for the entire range of investigated primary energies.

Apart from the width of ERF, the main disadvantage of the discussed fitting algorithm is represented by the position and exponential decay of inverse L'Hoir - its form spans from Gaussian peak to extremely prolonged shapes, as the MS regime becomes more profound with increasing of the primary energy of the probes. Moreover, the skewness of the peak influences its position as well. The position of the Gaussian peak, utilized for MS description, also caused an instability of the algorithm and had to be empirically stabilized. The shape of the MS regime is, hence, unstable. In Sec. 2.3, further discussion is provided.

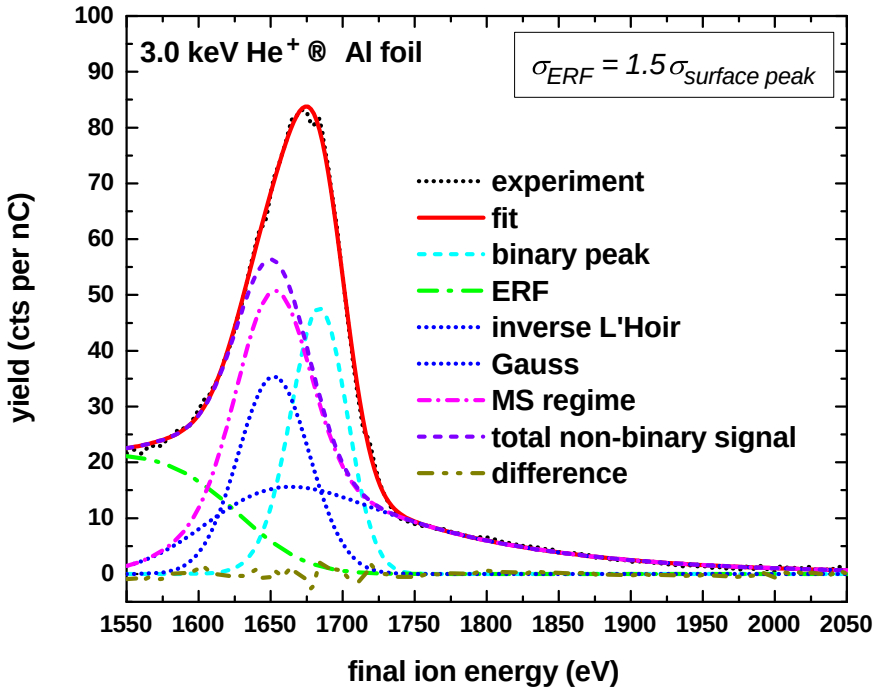

Figure 2.10: Result of the fitting algorithm for 3.0 keV He^+ projectiles on Al foil with $\sigma_{ERF} = 1.5\sigma_{surface\,peak}$. The agreement between the experiment and the fit for the MS regime is perfect. Small discrepancy can be observed around 1550 eV.

2.2.7 Comparison of Van Cittert deconvolution and Multiple-scattering approach

Presented spectra offer a possibility to discuss the results of the deconvolution process further. Opting for the L'Hoir peak in the case of 3.0 keV He^+ projectiles, a good agreement between MS approach, with $\sigma_{ERF} = 1.5 \cdot \sigma_{surface\,peak}$, and deconvolution algorithm with

L'Hoir response, $\tau = 0.75 \cdot \sigma_{surface\,peak}$, was found, as compared in Fig. 2.11. The binary peak, predicted by deconvolution, has slightly larger skewness than the one obtained via the MS approach. Utilizing the deconvolution algorithm for the entire energy range is not presented in this work, since the requirement of manual tuning of governing parameters for the successful fits, namely skewness and width of the L'Hoir peak, would not provide a controlled enviroment for the resulting integrals of the binary peaks. Moreover, in order to eliminate the drop of the background near the high energy edge of the binary peak, many combinations of τ and σ can be found. In addition, suppression of this drop is, in the current state of affairs, subjective. Hence the boundary condition, establishing when the drop has been eliminated, would be required.

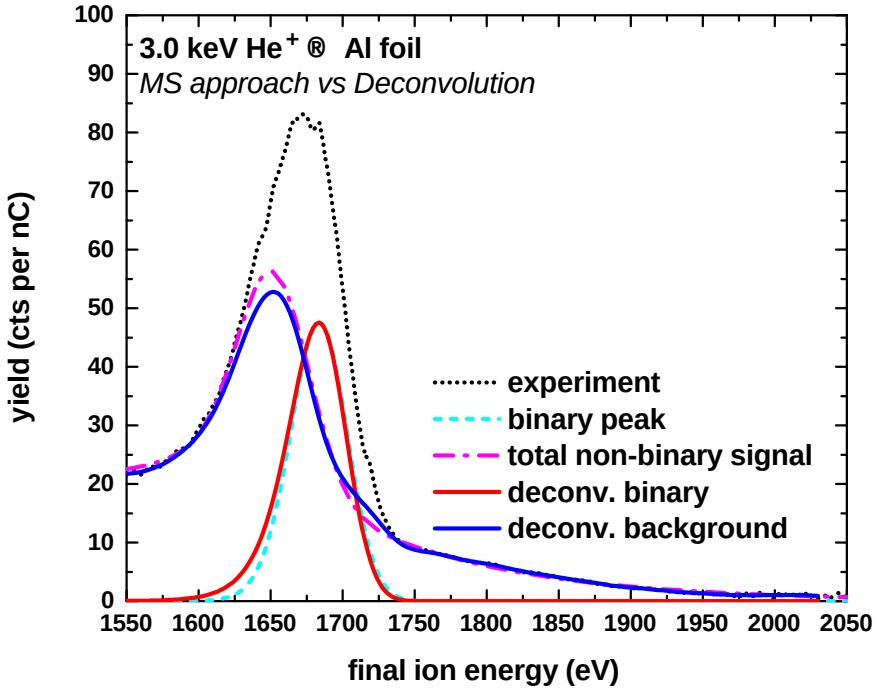

Figure 2.11: Comparison of MS approach and deconvolution for 3.0 keV He^+ projectiles. For Van Cittert deconvolution, L'Hoir peak with $\tau = 0.75 \cdot \sigma_{surface\,peak}$ was chosen as a response function. Discrepancy between MS approach (magenta dash-dot) and deconvolution (blue solid) background is not extreme, considering the fact that two completely different approaches were executed in order to fit the experimental (black dot) spectrum.

2.3 Results of fitting methods

To begin with, the first two mentioned approaches, a combination of either Gaussian or L'Hoir peak with the ERF are discussed. The integral curves are the results of the evaluation of the area of the binary peak, obtained for He^+ projectiles impinging on Al foil for primary energies ranging from 1.0 keV to 4.8 keV. Since the position and width of ERF were kept constant for both fitting methods, the integrals of binary peak remain, practically, identical.

Applying the MS approach, the shape of the integral curve changes significantly and resembles the shape of He^+ projectiles on silver. These results are shown in Fig. 2.12 . Red data (MS approach for Al) were multiplied by constant to match the area below the black curve (L'Hoir + ERF, He^+ on Ag (100)). Blue data (L'Hoir + ERF for Al) are

multiplied by a constant for sole comparative purposes to show the difference between the two approaches and match the value of integral for 1.0 keV He^+ on Ag (100).

The difference between blue and red curves indicates that the ion fraction P_i^+ ((Eq. 1.18)) as a function of energy has either a similar dependence as for Ag (red curve), or it behaves in a completely different (blue curve) manner.

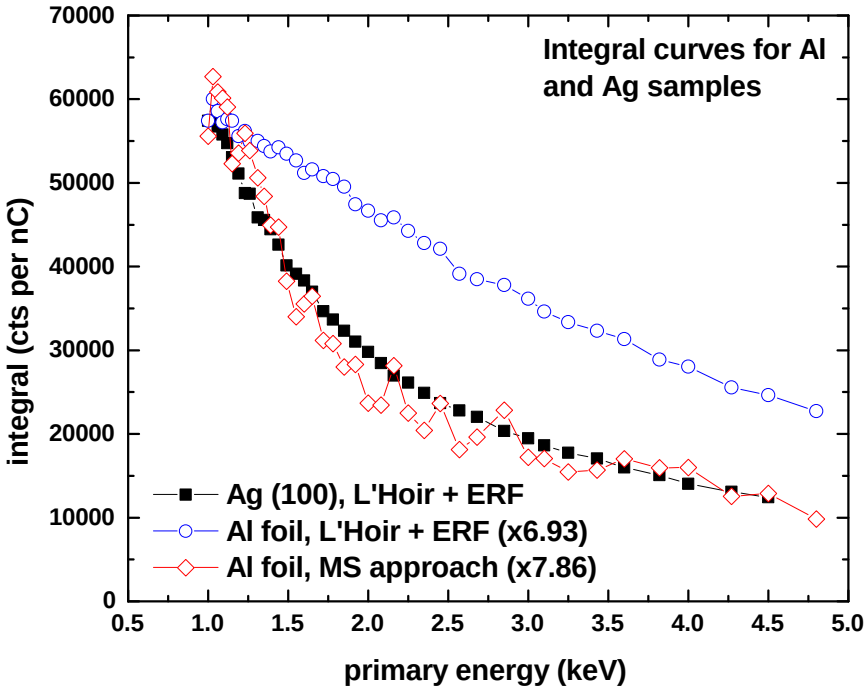

Figure 2.12: Integrals for Al foil, L'Hoir + ERF (blue open circles) and MS approach (red open diamonds). The latter results in a similar shape to L'Hoir + ERF applied on Ag (100) crystal (black squares). According to the choice of fitting method, an integral curve for Al foil either follows the shape of an integral curve for Ag (100), or deviates significantly. If the first fitting method, the MS approach, approximates real experiments correctly, the P_i^+ has very similar energy dependance on the primary energy for both samples, different only in magnitude. If the other fitting approach, L'Hoir + ERF, corresponds closer with the reality, P_i^+ parameter differs significantly for presented samples. Lines in the data are added in order to lead the eye.

Improvement, represented by the residual sum of squares, in agreement between the experimental data and the fit for discussed descriptions of LEIS data, applied on He^+ on Al foil, is shown in Tab. 2.1 and Fig. 2.13. For the area of interest, the part of the spectrum between the inflex points from both sides of the surface peak, as discussed in Sec. 2.1, was chosen. Interestingly, the RSS is decreasing with primary energy in the range from 1.0 keV to 1.09 keV. This trend is observed for all three cases. The combination of Gauss + ERF yields the most inaccurate fits, as expected. Utilizing the L'Hoir + ERF method, an abrupt improvement, compared to the Gaussian description of binary peak, is observed, with the exception of the lowest primary energies, from 1.0 keV to 1.26 keV, when its values are comparable (mutual ratio up to 0.65) with the Gaussian results.

	RSS (cts^2)			Ratio	
E_0 (keV)	Gauss	L'Hoir	MS approach	L'Hoir / Gauss	MS approach / L'Hoir
1.0	3423.2	2104.5	645.3	0.615	0.307
2.0	12507.1	1923.2	238.1	0.154	0.124
3.0	6750.8	1094.8	70.2	0.162	0.064
4.0	2519.9	399.6	69.8	0.159	0.175

Table 2.1: Comparison of RSS for different evaluation methods. MS approach results in significantly closer agreement with the experimental data.

The MS approach finds the best agreements in the area of interest between the experiments and the fits. It is, on average, almost 6.6 times more accurate than the L'Hoir + ERF fitting procedure. With small exceptions, it has a decreasing trend for the entire range of investigated primary energies. An interesting, abrupt improvement of the fits, is observed between 2.85 keV and 3.6 keV of primary energies.

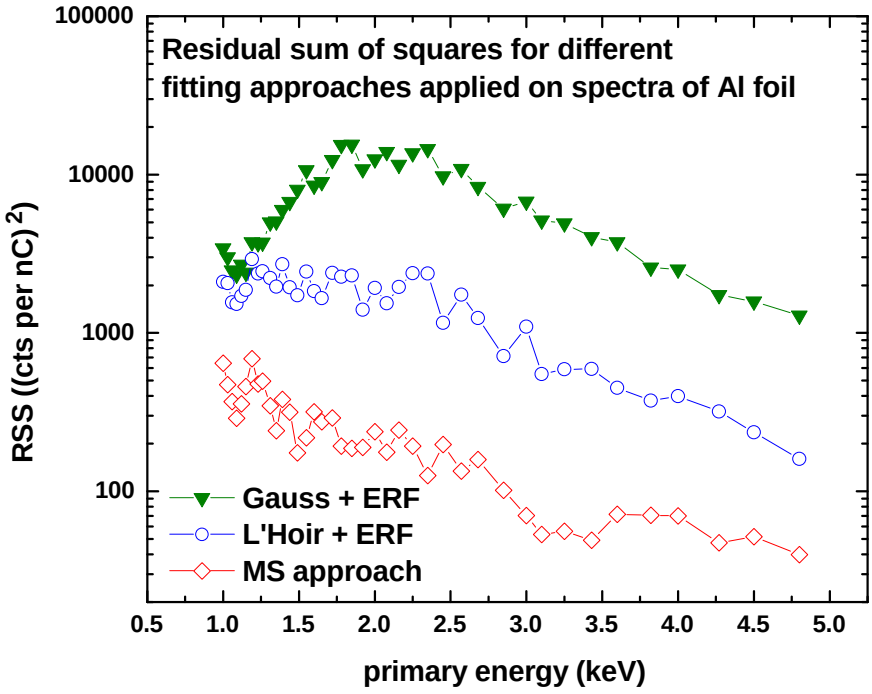

Figure 2.13: Residual Sum of Squares analysis applied on integral curves for respected methods applied on spectra for Al foil. The y-axis is in logarithmic scale. A combination of Gauss + ERF (green triangles) yields the largest discrepancy between the experiment and the fit. Substituting Gauss by L'Hoir, agreement abruptly improves (blue open circles). Finally, the MS approach (red open diamonds) manages to describe the experimental data with the highest precision. Lines in the data are added in order to lead the eye.

Conclusion

In the presented work, a description of the LEIS experiments, collected by an electrostatic analyzer, was investigated. For the analysis, spectra for aluminium foil were chosen, since aluminium has only one naturally occurring stable isotope. Fitting methods were implemented on spectra with He^+ projectiles with primary energies ranging from 1.0 keV to 4.8 keV. All data were collected by IONTOF Qtac^{100} system.

First, a standard fitting procedure for LEIS spectra, combining the Gaussian function (binary peak) and Error function (background from both sides of the surface peak), has been described. To find a better agreement between the fit and the experimental data, the Gaussian function was substituted by the L'Hoir peak. In both fitting procedures, the area of the surface peak is described, mostly, by binary peak. While both approaches are robust and produce stable and, practically, identical results, they do not include the theoretical description and the magnitude of different scattering mechanisms contributing to the final shape of the surface peak. For this reason, a parallel investigation by TRBS simulations and Van Cittert (- Jannson) deconvolution algorithm has been conducted. In principle, both approaches predict a similar qualitative outcome: for spectra with the visible multiple-scattering regime, the area of the surface peak should not be described, predominantly, by the binary peak, since a strong contribution of the multiple-scattering regime is possible.

Taking these results into consideration, an alternative fitting algorithm has been proposed. The multiple-scattering regime is approximated by the mutual combination of the Gauss function and inverse L'Hoir peak. This idea originated from the observations of TRBS results when contributions of different collisional regimes to the final shape of the spectrum were investigated. The binary peak is described by the L'Hoir peak. For fitting of the reionized background, the Error function is kept. Therefore, reionized background and multiple-scattering regimes are no longer described by a single function (Error function), but the fitting procedure treats them separately. For this reason, we have denoted this fitting procedure as a Multiple-scattering approach.

The discussed approach provides the closest agreement between the experiment and the fit. On the other hand, the energy dependence of the integrals of binary peaks for the investigated range of primary energies is noisy, when compared to previous, robust fitting procedures. Due to the multitude of fitting parameters and a requirement of certain boundary conditions to be kept loose in order to find a reasonable agreement in the entire range of investigated energies, the MS approach is fragile.

Bibliography

[1] Brongersma, H., Draxler, M., de Ridder, M., and Bauer, P. Surface composition analysis by low-energy ion scattering. *Surface Science Reports*, 62 (3), **2007**, pp. 63–109.

[2] Zhou, W., Zhu, H., and Yarmoff, J. A. Termination of single-crystal Bi_2Se_3 surfaces prepared by various methods. *Phys Rev B*, 94, **2016**, p. 195408.

[3] Roth, D., Goebl, D., Primetzhofer, D., and Bauer, P. A procedure to determine electronic energy loss from relative measurements with TOF-LEIS. *Nuclear Instruments and Methods in Physics Research Section B: Beam Interactions with Materials and Atoms*, 317, **2013**, pp. 61–65.

[4] Koslowski, H. R., Schmitz, J., and Linsmeier, C. Temporally resolved LEIS measurements of Cr segregation after preferential sputtering of WCrY alloy. *Nuclear Instruments and Methods in Physics Research Section B: Beam Interactions with Materials and Atoms*, 479, **2020**, pp. 42–46.

[5] Rabalais, J. W. *Principles and Applications of Ion Scattering Spectrometry: Surface Chemical and Structural Analysis*. ISBN: 978-0-471-20277-6a, **2002**.

[6] Walls, J. *Methods of surface analysis: techniques and applications*. CUP Archive, **1990**.

[7] Alford, T. L., Feldman, L. C., and Mayer, J. W. *Fundamentals of nanoscale film analysis*. Springer Science & Business Media, **2007**.

[8] Sigmund, P. and Winterbon, K. Small-angle multiple scattering of ions in the screened Coulomb region: I. Angular distributions. *Nuclear Instruments and Methods*, 119, **1974**, pp. 541–557.

[9] Biersack, J. and Ziegler, J. The stopping and range of ions in solids. In *Ion Implantation Techniques: Lectures given at the Ion Implantation School in Connection with Fourth International Conference on Ion Implantation: Equipment and Techniques Berchtesgaden, Fed. Rep. of Germany, September 13–15, 1982*, pp. 122–156. Springer, **1982**.

[10] Grande, P. L. and Schiwietz, G. Impact-parameter dependence of electronic energy loss and straggling of incident bare ions on H and He atoms by using the coupled-channel method. *Physical Review A*, 44 (5), **1991**, p. 2984.

[11] Průša, S., *et al.* A practical guide to interpreting low energy ion scattering (LEIS) spectra. *Applied Surface Science*, 657, **2024**, p. 158793.

[12] Cortenraad, R., *et al.* Crystal-face dependence of low-energy ion scattering signals. *Nuclear Instruments and Methods in Physics Research Section B: Beam Interactions with Materials and Atoms*, 174 (1-2), **2001**, pp. 173–180.

[13] Primetzhofer, D., Spitz, M., Taglauer, E., and Bauer, P. Resonant charge transfer in low-energy ion scattering: Information depth in the reionization regime. *Surface science*, 605 (21-22), **2011**, pp. 1913–1917.

[14] Prusa, S., *et al.* Calcium and fluorine signals in HS-LEIS for CaF2 (111) and powder—Quantification of atomic surface concentrations using LiF (001), Ca, and Cu references. *Surface Science Spectra*, 27 (2), **2020**.

[15] Goebl, D., Bruckner, B., Roth, D., Ahamer, C., and Bauer, P. Low-energy ion scattering: A quantitative method? *Nuclear Instruments and Methods in Physics Research Section B: Beam Interactions with Materials and Atoms*, 354, **2015**, pp. 3–8.

[16] Rund, S., Primetzhofer, D., Markin, S., Goebl, D., and Bauer, P. Charge exchange of He+-ions with aluminium surfaces. *Nuclear Instruments and Methods in Physics Research Section B: Beam Interactions with Materials and Atoms*, 269 (11), **2011**, pp. 1171–1174.

[17] Cushman, C. V., *et al.* Low energy ion scattering (LEIS). A practical introduction to its theory, instrumentation, and applications. *Analytical Methods*, 8 (17), **2016**, pp. 3419–3439.

[18] Lin, Y., Wu, Z., Wen, J., Poeppelmeier, K. R., and Marks, L. D. Imaging the atomic surface structures of CeO2 nanoparticles. *Nano letters*, 14 (1), **2014**, pp. 191–196.

[19] Biersack, J., Steinbauer, E., and Bauer, P. A particularly fast TRIM version for ion backscattering and high energy ion implantation. *Nuclear Instruments and Methods in Physics Research Section B: Beam Interactions with Materials and Atoms*, 61 (1), **1991**, pp. 77–82.

[20] Draxler, M., *et al.* Explanation of the surface peak in charge integrated LEIS spectra. *Nuclear Instruments and Methods in Physics Research Section B: Beam Interactions with Materials and Atoms*, 203, **2003**, pp. 218–224.

[21] Ter Veen, H., Kim, T., Wachs, I., and Brongersma, H. Applications of high sensitivity-low energy ion scattering (HS-LEIS) in heterogeneous catalysis. *Catalysis Today*, 140 (3-4), **2009**, pp. 197–201.

[22] Limburg, J., *et al.* Energy loss of keV He2+ scattered off an A1 (110) surface. *Surface science*, 409 (3), **1998**, pp. 541–552.

[23] Lang, N. D. *The density-functional formalism and the electronic structure of metal surfaces*, vol. 28. Elsevier, **1974**, pp. 225–300.

[24] Närmann, A., *et al.* Charge exchange and energy dissipation of particles interacting with metal surfaces. *Physical review letters*, 64 (13), **1990**, p. 1601.

[25] Li, T. and MacDonald, R. Inelastic energy loss and charge exchange in low-energy heavy ions scattered from Cu and Cu-alloy surfaces. *Physical Review B*, 51 (24), **1995**, p. 17876.

[26] L'Hoir, A. Study of the asymmetrical response of silicon surface barrier detectors to MeV light ions. Application to the precise analysis of light ions energy spectra I. Helium ions. *Nuclear Instruments and Methods in Physics Research*, 223 (2-3), **1984**, pp. 336–345.

[27] Marzo, G. A. A comparison of different peak shapes for deconvolution of alpha-particle spectra. *Nuclear Instruments and Methods in Physics Research Section A: Accelerators, Spectrometers, Detectors and Associated Equipment*, 832, **2016**, pp. 191–201.

[28] Van Cittert, P. Zum einfluss der spaltbreite auf die intensitätsverteilung in spektrallinien. ii. *Zeitschrift für Physik*, 69 (5), **1931**, pp. 298–308.

[29] Jansson, P. A., Hunt, R. H., and Plyler, E. K. Resolution enhancement of spectra. *JOSA*, 60 (5), **1970**, pp. 596–599.

[30] Markin, S., Primetzhofer, D., Valdés, J., Taglauer, E., and Bauer, P. Neutralization of low energy He+ ions by Cu in the Auger regime. *Nuclear Instruments and Methods in Physics Research Section B: Beam Interactions with Materials and Atoms*, 258 (1), **2007**, pp. 18–20.

[31] Goldberg, E., Monreal, R., Flores, F., Brongersma, H., and Bauer, P. New model for ion neutralization at surfaces. *Surface science*, 440 (3), **1999**, pp. L875–L880.

[32] Bruckner, B., Strapko, T., Sortica, M. A., Bauer, P., and Primetzhofer, D. On the influence of uncertainties in scattering potentials on quantitative analysis using keV ions. *Nuclear Instruments and Methods in Physics Research Section B: Beam Interactions with Materials and Atoms*, 470, **2020**, pp. 21–27.

Curriculum vitae

Ing. Tomáš Strapko

Address: Bottova 992/7, 921 01 Piešťany, Slovenská republika
E-mail: 170450@vutbr.cz

Education

2019 - now doctoral studies, Institute of Physical Engineering, Physical and Material Engineering, Brno University of Technology

2017 - 2019 master studies, Institute of Physical Engineering, Physical Engineering and Nanotechnologies, Brno University of Technology

2014 - 2017 bachelor studies, Institute of Physical Engineering, Physical Engineering and Nanotechnologies, Brno University of Technology

Working experience

2022 - now Activair, s.r.o.; R&D; vacuum technologies

Languages

Slovak native speaker
Czech passive user
English level C1
German level A1

Hobbies

fencing, chess, swimming, reading